

Study of the electron-phonon interaction in metal diborides MeB₂ (Me=Zr, Nb, Ta, Mg) by point-contact spectroscopy

I. K. Yanson¹, Yu. G. Naidyuk¹, O. E. Kvitnitskaya¹, V. V. Fisun¹, N. L. Bobrov¹, P. N. Chubov¹, V. V. Ryabovol¹, G. Behr², W. N. Kang³, E.-M. Choi³, H.-J. Kim³, S.-I. Lee³, T. Aizawa⁴, S. Otani⁴, and S.-L. Drechsler²

¹ *B. Verkin Institute for Low Temperature Physics and Engineering,*

National Academy of Sciences of Ukraine, 47 Lenin Ave., 61103, Kharkiv, Ukraine

² *Leibniz-Institut für Festkörper- und Werkstofforschung Dresden e.V., Postfach 270116, D-01171 Dresden, Germany*

³ *Pohang University of Science and Technology, Pohang 790-784, South Korea and*

⁴ *Advanced Materials Lab., National Institute for Materials Sciences, 1-1 Namiki, Tsukuba, Ibaraki 305-0044, Japan*

(Dated: October 26, 2018)

We review investigations of the electron-phonon interaction (EPI) in metal diborides MeB₂ (Me=Zr, Nb, Ta, Mg) by point-contact (PC) spectroscopy. For transition metal compounds the PC EPI functions were recovered and EPI parameter $\lambda \lesssim 0.1$ were estimated. The data are consistent with the measured surface phonon dispersion curves. The low λ value questions some reports about superconductivity in these compounds. Contrary, EPI in superconducting MgB₂ films manifests also in the PC spectra itself by virtue of an elastic EPI contribution to the excess current determined by the energy dependence of the superconducting order parameter. To analyse the phonon features in the PC spectra of MgB₂ a two-band model is exploited and the proximity effect in the \mathbf{k} -space is suggested.

PACS numbers: 63.20.Kr, 74.80.Fp, 73.40.Jn

Introduction. Recently discovered superconductivity in the *sp* compound MgB₂¹ attracts much attention mainly due to relatively high $T_c \simeq 39$ K, which is the highest as for two-component systems. Probably a specific feature of this compound appears to be a rare example of two disconnected bands of the Fermi surface with quite different dynamical properties^{2,3,4}. One of those bands is two-dimensional (2D), with extremely strong electron-phonon interaction (EPI), while the other is 3D with a weak EPI^{3,4,5,6}.

The overwhelming majority of the community anticipated an electron-phonon mechanism in MgB₂^{4,5,6,7,8}. Thus, the preferable reason of the formation of Cooper pairs is EPI, and its investigation to understand the nature and peculiarities of superconductivity in MgB₂ is vastly desirable.

In the wake of the finding of superconductivity in MgB₂ scientific activity was applied to its search in other diborides (all having a hexagonal layered crystal structure of an AlB₂ type) along with the further study of their properties. According to a recent review⁹ no superconducting transition has been observed so far in the diborides of transition metals MeB₂ (Me=Ti, Zr, Hf, V, Cr, Mo). As to the superconductivity in NbB₂, TaB₂ and ZrB₂ controversial reports can be found^{9,10}.

In this article we would like to summarize our findings in the determination of the EPI function for the above mentioned diborides from the point-contact (PC) spectra. The attractive feature of the PC spectroscopy is that the measurement at low temperatures of the voltage derivative of the PC resistance allows a straightforward determination¹¹ of the PC EPI function $\alpha^2 F(\omega)$. The knowledge of $\alpha^2 F(\omega)$ for conducting systems provides a consistent check for the possibility of a phonon-mediated pairing mechanism, e.g., by estimation of the electron-

phonon-coupling strength characterized by the EPI parameter $\lambda = 2 \int \alpha^2 F(\omega) \omega^{-1} d\omega$. From the comparison of the experimentally determined $\alpha^2 F(\omega)$ with theoretical calculations different models and approaches can be discriminated.

Experimental details. The samples are *c*-axis oriented films of MgB₂, whose characteristics are described in Ref.¹² and single crystals of MeB₂ (Me=Zr, Nb, Ta). The residual resistivity ρ_0 and the residual resistivity ratio (RRR) of all investigated diborides are shown in Table 1.

Different PC's were established *in situ* by touching of the MgB₂ film or the cleaved surface of a transition metal single crystal by a sharpened edge of an Ag counterelectrode. This geometry corresponds to a current flowing preferably along the *c*-axis of the film. A number of contacts was measured by touching the film edge after breaking Al₂O₃ substrate. By this means, the current flows preferably along the *ab* plane. As to PC's on another diborides, the orientation of electrodes was not controlled with respect to the crystallographic axis. The zero-bias resistance R_0 of the investigated contacts ranged from a few ohms up to several tens of ohms at 4.2 K.

Both the differential resistance dV/dI and the second derivative of $I - V$ characteristic $d^2V/dI^2(V)$ vs V were registered using a standard lock-in technique.

Results and discussion. According to the Kulik, Omelyanchouk and Shekhter theory¹³ the second derivative $-d^2I/dV^2(V)$ of the $I - V$ curve of a ballistic PC at low temperatures due to EPI is proportional to $\alpha_{PC}^2 F(\omega)$. In the free electron approximation¹⁴

$$-\frac{d^2I}{dV^2} \propto R^{-1} \frac{dR}{dV} = \frac{8ed}{3\hbar v_F} \alpha_{PC}^2(\epsilon) F(\epsilon)|_{\epsilon=eV}, \quad (1)$$

where $R = dV/dI$. The factor $K = 1/2(1 - \theta/\tan \theta)$, entering in α_{PC}^2 , takes into account the kinematic restric-

TABLE I: Parameters of investigated diborides.

Compound	Sample	$\rho_0 \cdot 10^9, \Omega \text{ m}$	RRR	$n^a \cdot 10^{-28}, \text{ m}^{-3}$
MgB ₂	film	60	2.3	6.9
ZrB ₂	sgl. cry.	3.3	24	13
NbB ₂	sgl. cry.	-	-	18.2
TaB ₂	sgl. cry.	220	1.2	18.6

^a The density of carriers n was estimated by the number of valence electrons (2 for MgB₂, 4 for ZrB₂, 5 for NbB₂ and TaB₂) per volume of the corresponding unit cell.

tion of electron scattering processes in PC (for transport and Eliashberg EPI functions the corresponding factors are: $K = (1 - \cos \theta)$ and $K=1$, respectively, with θ is the angle between initial and final momenta of scattered electrons). Respectively, the large angle $\theta \rightarrow \pi$ scattering (back-scattering) processes of electrons dominate in α_{PC}^2 .

According to Eq.(1) the measured rms signal of the first V_1 and second V_2 harmonics of a small alternating voltage superimposed on the ramped dc voltage V defines the EPI function $\alpha_{PC}^2(\epsilon) F(\epsilon)$:

$$\alpha_{PC}^2(\epsilon) F(\epsilon) = \frac{3\sqrt{2} \hbar v_F V_2}{4 ed V_1^2}. \quad (2)$$

To estimate the PC diameter d , which enters in Eqs.(1) and (2), the relation $R_{PC}(T) \simeq \frac{16\rho l}{3\pi d^2} + \frac{\rho(T)}{d}$ derived by Wexler¹⁵ is commonly used, which consists of a sum of the ballistic, Sharvin, and the diffusive, Maxwell, terms. Here $\rho l = p_F/ne^2$, where p_F is the Fermi momentum, n is the density of charge carriers.

A. Transition metal diborides

Representative examples of the $d^2I/dV^2(V)$ dependencies for each compound averaged over both voltage polarities are shown in Fig. 1 (left panel). Reproducible phonon maxima are clearly resolved up to 100 mV (see ZrB₂), while for TaB₂ only low energy peak at 20 mV is seen. The spectra exhibit also a zero-bias anomaly, especially remarkable in NbB₂ and TaB₂. A common feature for all spectra is the presence of the main low-energy maximum placed at about 30, 28 and 20 mV for ZrB₂, NbB₂ and TaB₂, respectively. This is in line with the general consideration that at fixed spring constants the phonon frequency decreases with increasing of atomic mass (see Fig. 1, right panel). Such a behavior suggests that the first peak corresponds to the vibration of the transition metal. On the other hand the neutron data peak position for MgB₂ on Fig. 1 (right panel) at about 35 meV¹⁶ is far below the straight line connecting the MeB₂ compounds. This might be considered as the consequence of a softening of the corresponding spring constants (i. e. metallic bonds in MgB₂ instead of relatively strong MeB₂ covalent bonds in the MeB₂ series).

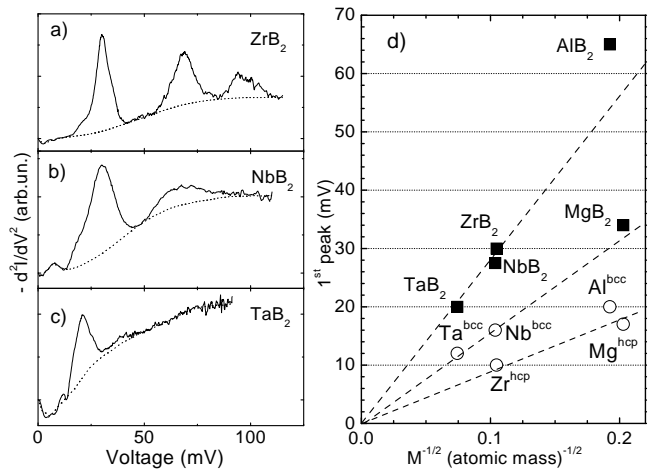


FIG. 1: Left panel: PC spectra $-d^2I(V)/dV^2 \propto d^2V/dI^2(dV/dI)^{-3}$ for investigated compounds at $T = 4.2\text{K}$. The dashed curves represent background behavior. The zero-bias resistance and modulation signal are for ZrB₂: $R_0 = 5.5 \Omega$, $V_1(0)=0.8 \text{ mV}$; for NbB₂: $R_0 = 50 \Omega$, $V_1(0)=2.8 \text{ mV}$; for TaB₂: $R_0 = 25 \Omega$, $V_1(0)=1.3 \text{ mV}$. Right panel: The position of the first peak (squares) in the measured spectra for ZrB₂, NbB₂ and TaB₂ vs the inverse square root of atomic mass of the transition metals. For MgB₂ and AlB₂ the peak position is according to the inelastic neutron scattering data¹⁶. Open circles show the position of the first peak in the PC spectra for the corresponding metals^{17,18}. Straight dashed lines are guide to eye.

Fig. 2 presents the recovered PC EPI functions (top panel) for the investigated diborides ZrB₂ and NbB₂ calculated by Eq.(2) along with the High Resolution Electron-Energy-Loss Spectroscopy (HREELS) data¹⁹ for surface phonon dispersion (bottom panel). Details of the reconstruction of the PC EPI functions according to Eq.(2) are described in Ref.²⁰.

Because of the large mass difference between the transition metal and the boron atoms and strong covalent B-B bonds the boron modes are expected at much higher energy. For ZrB₂ two additional maxima at 70 and 100 mV are well resolved, while for NbB₂ the high energy part of the spectrum presents a broad maximum around

TABLE II: The phonon maxima and the EPI constant λ in MeB₂ compounds measured by PC spectroscopy. The fifth column shows the maximal energy for phonon features in the PC spectrum^{17,18} for the corresponding transition metals: Me=Zr, Nb, Ta.

Samples	1 st peak	2 nd peak	3 ^d peak	$\hbar\omega_{max}^T$	λ_{PC}
	meV	meV	meV	meV	
MgB ₂	30(?)	~ 60	~ 90	30	-
ZrB ₂	30 ± 0.5	68 ± 1	94 ± 2	25	0.06
NbB ₂	28 ± 2	60 ± 5	-	28	0.08
TaB ₂	20 ± 1	40(?)	-	20	0.025

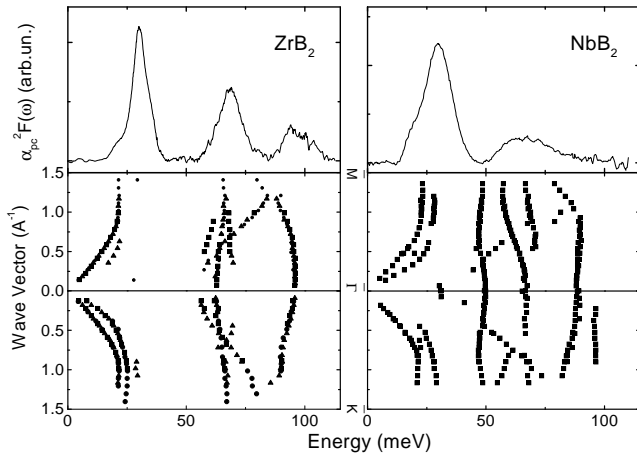


FIG. 2: The PC EPI function for ZrB_2 and NbB_2 recovered from the spectra in Fig. 1. (top panel) as compared to the HREELS data for these compounds¹⁹ (bottom panel).

60 mV. For TaB_2 the high energy phonon peaks were difficult to resolve, where according to a rough estimation²¹ the boron in-plane and out of plane displacement modes should have energies of 98 and 85 meV, respectively. No spectral features were found for the mentioned compounds above 100 meV. Our spectra are in line with the measured surface phonons¹⁹ for ZrB_2 and NbB_2 although the surface phonons, in general, are softer. For both compounds phonon dispersion study¹⁹ (Fig. 2, bottom panel) demonstrates a gap between 30-50 meV which separates acoustic and optic branches. Close to this energy region a minimum in our PC spectra occurs. Comparing the high energy parts of the ZrB_2 and NbB_2 PC spectra, we may support the statement¹⁹, that for NbB_2 the boron surface phonon modes are softer and more stretched than in the case of ZrB_2 giving rise to structureless maxima around 60-70 mV (see Fig. 1). Note that the upper boundaries of the ZrB_2 and NbB_2 PC spectra are at about 110 mV and 90 mV (see Fig. 1), what is much larger than their Debye temperatures of 280 K and 460 K, respectively, estimated from the Bloch-Grüneisen temperature dependence of the resistivity¹⁰.

With the use of the EPI function the parameter $\lambda = 2 \int \alpha^2 F(\omega) \omega^{-1} d\omega$ was calculated. For many superconductors it was found¹⁸ that $\lambda_{\text{PC}} \simeq \lambda_{\text{Eliashberg}}$. Table 2 shows that λ_{PC} is rather low for the investigated diborides what is in line with the small λ values reported for PC studies of the transition metal silicides NbSi_2 and TaSi_2 ²² ($\lambda_{\text{PC}} \simeq 0.02$). The possible reasons for a small λ value are discussed in Ref.²⁰. Our results show that NbB_2 has the largest λ_{PC} among the studied compounds, therefore existence of superconductivity in NbB_2 with observable T_c is more likely.

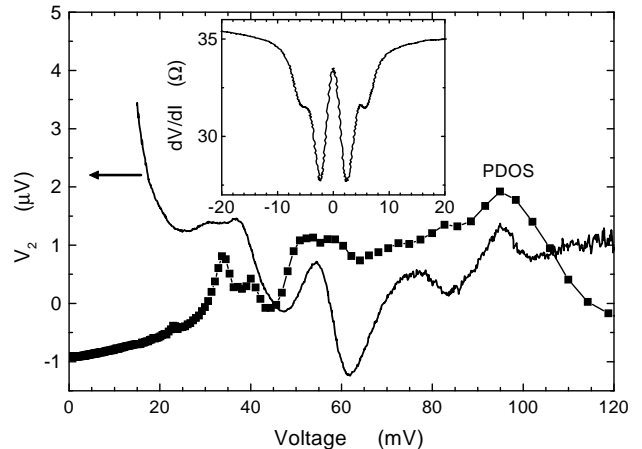


FIG. 3: Averaged for both polarities spectrum $V_2 \propto d^2V/dI^2$ after subtracting of a linear background of MgB_2 -Ag PC ($R_0 = 35 \Omega$, $T=4.2 \text{ K}$, $V_1(0)=2.52 \text{ mV}$) in comparison to the neutron PDOS of MgB_2 ¹⁶. Inset: differential resistance $R=dV/dI(V)$ of the same PC.

B. MgB_2

In Fig. 3 the $V_2 (eV) \propto d^2V/dI^2 (eV)$ and $dV/dI(V)$ (in the inset) characteristics are shown in the superconducting state at zero field. In the energy-gap region the two gap features are clearly seen with $\Delta_1 = 2.4$ and $\Delta_2 = 5.7$ meV (see inset). Further on, we simply denote by Δ the position of a dV/dI minimum. In Fig. 3 the $V_2(V) \propto d^2V/dI^2$ dependence after subtracting of linear background in comparison to the phonon density of states (PDOS)¹⁶ is shown. Some accordance is seen between the positions of PDOS peaks and maxima in $V_2(V)$ dependence.

The reproducibility of this kind of PC spectrum for different contacts is seen in Fig. 4(b). Here, the contact resistance varies from 43 to 111 Ω with gap minima at $\Delta = 2.1, 2.6,$ and 4.9 meV, respectively. The larger gap for curve 3 equals 7.0 meV. All the PC spectra (b) correlate with PDOS. The slight variation is probably due to the anisotropy and different scattering rates in the contacts. Compared with the theoretical EPI function for an isotropic one-band model (see, for example, Ref.^{5,6,8}), the peak at $eV=60 \div 70$ meV of E_{2g} boron mode is not too much higher in intensity, in accord with our earlier observation²³. For the two-band model in clean limit, we expect an information mostly from the 3D band keeping in mind that we measure the c-axis oriented films. In this case, the theory predicts, that the EPI spectral function has the E_{2g} -peak intensity of the same order of magnitude as the other peaks of PDOS (see Fig. 1 in Ref.²⁴).

According to our classification of the energy gap structure²⁵, it is due to the random orientation of the contact axis and scattering of charge carriers between two-band of Fermi surface, having gaps Δ_1 and Δ_2

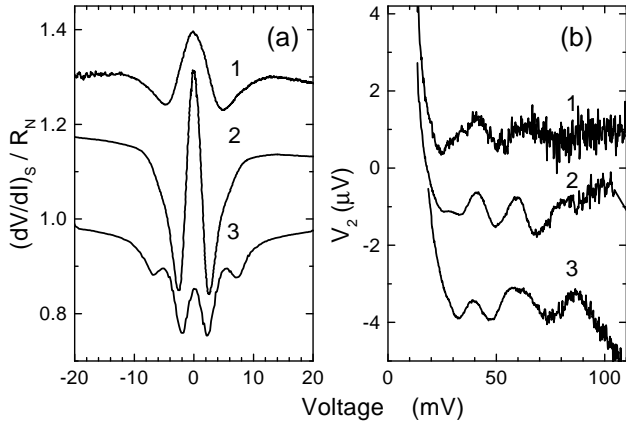


FIG. 4: (a) Normalized to the normal state (at $V \simeq 30$ mV) differential resistance at $T=4.2$ K for 3 PC's with $R_0=111$, 43, and 45 Ω (curves 1-3 respectively). Curves 1,2 are shifted for clarity. (b) Second harmonic signal V_2 with modulation voltages $V_1(0)=2.5$, 2.78, and 3.31 mV, respectively for same PC's.

mixed. With an increase of interband scattering the magnitude of Δ_1 (Δ_2) moves to the higher (lower) value, respectively. For dirty contacts, where the admixture of the 2D band is essential, only one gap maximum remains with a broad distribution around $\simeq 3.5$ meV²⁵. In this case l is smaller than d (where l and d are the electron mean free path and the size of the contact, respectively), and the inelastic backscattering contribution to the phonon structure, proportional to l/d^{26} , is small. Therefore, in the superconducting state, the observed phonon structure presents mainly the elastic contribution to the excess current²⁷. The elastic term is proportional to the energy dependent part of the excess current I_{exc} (eV), similar to the phonon structure in the quasi-particle DOS for tunneling spectroscopy^{27,28}:

$$\frac{dI_{exc}}{dV}(eV) = \frac{1}{R_0} \left| \frac{\Delta_{in}(eV)}{eV + \sqrt{(eV)^2 - \Delta_{in}^2(eV)}} \right|^2, \quad (3)$$

where $\Delta_{in}(eV)$ is the gap parameter in the 3D band, induced by the 2D-band EPI. As seen in Fig. 4(a), if the Δ value increases (curves 1-3), then the intensity of the phonon structure in the units of $d(\ln R)/dV = 2\sqrt{2}V_2/V_1^2$ increases too (Fig. 4(b)). That is because the modulation voltage V_1 decreases, whereas the amplitudes in $V_2(eV)$ -units remain approximately the same. Note, that for curve 3 in Fig. 4(a) one has to take the lower gap Δ_1 , because the current is mainly determined by 3D band, as mentioned above.

In Fig. 5, the normal state spectrum above T_c is displayed together with the differential resistances in the superconducting state (see inset), showing the energy

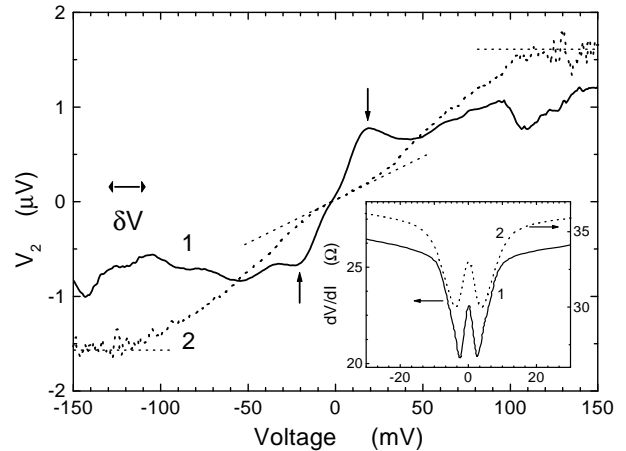


FIG. 5: Normal state spectra of MgB₂-Cu PC's taken at 41 K with $V_1(0)=2.2$ mV. For spectrum No.1 vertical arrows mark the low frequency bumps at about 20 mV. The horizontal double arrow bar stands for thermal smearing, determining the spectral resolution δV .

gap structure. In spite of an increase of the temperature smearing above 20 mV at 41 K the residual phonon structure is still visible (curve 1 in Fig. 5). The smeared phonon features are superimposed on the rising linear background. For curve 2, we see an increase in scattering at $\simeq 35$ mV, where the acoustic phonon peak occurs, and the saturation around 100 mV, where the phonon spectrum ends. In the normal state, only those nonlinearities remain, which are due to the inelastic processes¹³. We stress that judging from the larger superconducting gap value ($\simeq 3.5$ meV for curve 2 in the inset) the essential contribution is expected from the $\Delta_2(E)$ of 2D band for normal-state spectrum No.2. This spectrum should contrast with curve 6 in Fig. 6 (see below), where the direct contribution from the 2D band is small, due to lower value of Δ . Thus, the backscattering processes from the 3D band are mostly essential for spectrum 6 and the phonon features are not resolved at high energies. The shape of spectrum 1 in Fig. 5 presents the behavior intermediate between these two extremes, although its energy gap is approximately equal to curve 6 in Fig. 6. Beside the visible phonon features in the range 30 \div 100 mV, it possesses a low energy bump at about 20 mV.

The phonon spectra of PC with a small value of energy gaps are characterized by the presence of low frequency phonon peaks. The small peak at energy of about 25 mV (Fig. 6, curves 1, 2) is visible, where a tiny knee exists on the PDOS¹⁶ (see PDOS in Fig. 3). In the normal state (at $T \geq T_c$), these low frequency peaks transform into the S-shape structure in $d^2V/dI^2(V)$ spectra (curve 6), corresponding to the wide minimum of $dV/dI(V)$ near zero bias. This low-frequency structure is hardly due to the remnants of superconducting quasigap at $T > T_c$, since it is absent in junction No. 2, whose characteristic is

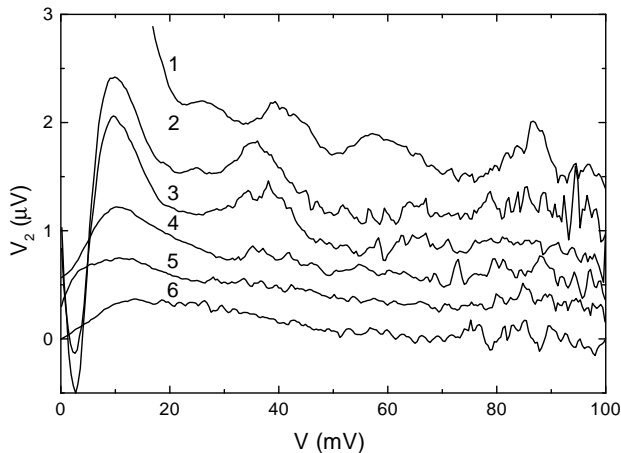


FIG. 6: Second harmonic dependences on field and temperature averaged for both voltage polarities. The temperature and magnetic field are: 4.2 K, 0 T; 4.2 K, 4 T; 10 K, 4 T; 20 K, 4 T; 30 K, 4 T; 40 K, 4 T, for curves 1-6, respectively. The modulation voltage $V_1(0)$ is 2.2 mV. $\Delta=2.7$ meV. Curves are shifted vertically for clarity.

shown in Fig. 5. Rather, it could be thought of as strong interaction in the 3D band with very low-frequency excitations, whose origin is not clear yet. On increasing the temperature, the low frequency peak broadens further like common spectral features do in the normal state.

Fig. 6 shows (compare curves 1 and 2) that the field smears out the intensity of the high energy peaks, which are induced in the 3D band by EPI of the 2D band. The disappearance of phonon peaks at field and temperature rise proves that they do not belong to the inelastic backscattering processes, which should have the same intensity both in the superconducting and in normal states. It seems more plausible that the high energy phonon peaks are due to the elastic contribution in the

excess current (3) induced by EPI from the 2D band, as was already stated above.

Conclusion. We have measured the PC spectra in transition metal diborides: ZrB_2 , NbB_2 and TaB_2 . For all compounds the main phonon peak position was established, the PC EPI function was recovered, and the EPI parameter λ was determined. The obtained small λ values question strongly the reported bulk superconductivity in these compounds with remarkable T_c . To draw a more weighty conclusion about details of EPI and the λ values in the presented MeB_2 family, a theoretical calculation of $\alpha_{PC}^2 F(\omega)$ with the mentioned K -factor and their comparison with experimental data is very desirable.

The PC EPI spectra of the superconducting MgB_2 differ even qualitatively from those measured for the mentioned transition-metals diborides. For MgB_2 the reproducible peaks on $d^2V/dI^2(V)$ are seen in the superconducting state, which disappear in the normal state. It proves that they are due to the energy dependence of the superconducting order parameter. The superconductivity here is presumably due to the 2D-band EPI, which induces the $\Delta(E)$ structure in the 3D band. At a small value of the superconducting gap the phonon structure is weak, and its intensity begins to increase with growing Δ . The robustness against the magnetic field also grows notably with increasing Δ .

In the normal state the intensity of the inelastic spectrum also correlates with the value of the superconducting gap. The tendency is observed that the high energy phonon contribution to the PC spectra becomes more prominent for a larger gap. This is supported also by our recent data on MgB_2 single crystals²⁹. For a smaller gap, the low-frequency bump appears in the spectra. It might be due to EPI with some unknown low-frequency excitation³⁰, but further work is needed to exclude that it is not caused simply by phonon peaks of the normal-metal counter electrode.

¹ J. Nagamatsu *et al.*, Nature (London) **410**, 63 (2001).
² S.V. Shulga *et al.*, cond-mat/0103154.
³ J. Kortus *et al.*, Phys. Rev. Lett **86**, 4656 (2001).
⁴ A.Y. Liu, I.I. Mazin, and J. Kortus, Phys. Rev. Lett. **87**, 087005 (2001).
⁵ Y. Kong *et al.*, Phys. Rev. B **64**, 020501(R) (2001).
⁶ T. Yildirim *et al.*, Phys. Rev. Lett, **87**, 037001 (2001).
⁷ H.J. Choi *et al.*, Phys. Rev B, **66**, 020513(R) (2002).
⁸ K.-P. Bohnen, R. Heid, and B. Renker, Phys. Rev. Lett. **86**, 5771 (2001).
⁹ C. Buzea and T. Yamashita, Superconductors, Science & Technology, **14**, R115-R146 (2001).
¹⁰ V. A. Gasparov *et al.*, JETP Lett. **73**, 532 (2001).
¹¹ I. K. Yanson, Sov. J. Low Temp. Phys. **9**, 343 (1983).
¹² W. N. Kang *et al.*, Science **292**, 1521 (2001); W.N. Kang *et al.*, Phys. Rev. Lett. **87**, 087002 (2001)
¹³ I. O. Kulik, A. N. Omelyanchouk and R. I. Shekhter, Sov.

J. Low Temp. Phys. **3** 840 (1977).
¹⁴ I. O. Kulik, Sov. J. Low Temp. Phys. **18**, 302 (1992).
¹⁵ A. Wexler, Proc. Phys. Soc. (London) **89**, 927 (1966).
¹⁶ B. Renker *et al.*, Phys. Rev. Lett **88**, 067001 (2002).
¹⁷ PC spectra of Zr were measured by N. L. Bobrov and V. V. Fisun (unpublished data).
¹⁸ A. V. Khotkevich and I. K. Yanson, *Atlas of Point Contact Spectra of Electron-Phonon Interaction in Metals* (Kluwer Academic Publisher, Boston, 1995).
¹⁹ T. Aizawa, W. Hayami, and S. Otani, Phys. Rev. B **65**, 024303 (2002).
²⁰ Yu. G. Naidyuk *et al.*, Phys. Rev. B **66** 140301(R) (2002).
²¹ H. Rosner *et al.*, Phys. Rev. B **64**, 144516 (2001).
²² O. P. Balkashin *et al.*, Sol. State Commun. **100**, 293 (1996).
²³ N. L. Bobrov *et al.*, in *New Trends in Superconductivity*, Vol.67 of NATO Advanced Studies Institute, Series B: *Physics and Chemistry*, edited by J.F. Annett and S. Kru-

- chinin, (Kluwer, Dordrecht, 2002), p.225.
- ²⁴ A. A. Golubov *et al.*, J. Phys.: Condens. Matter, **14**, 1353 (2002).
- ²⁵ Yu. G. Naidyuk *et al.*, JETP Letter **75**, 238 (2002).
- ²⁶ I. O. Kulik and I. K. Yanson, Sov. J. Low Temp. Phys. **4**, 596 (1978).
- ²⁷ I.K. Yanson, in *Quantum Mesoscopic Phenomena and Mesoscopic Devices in Microelectronics*, Vol.559 of NATO Science Series, Series C: Mathematical and Physical Sciences, edited by I.O. Kulik and R.Ellialtioglu, (Kluwer, Dordrecht, 2000), p. 61-77.
- ²⁸ A.N. Omel'yanchuk, S.I. Beloborod'ko and I.O. Kulik, Sov. J. Low Temp. Phys. **14**, 630 (1988).
- ²⁹ Yu. G. Naidyuk *et al.*, cond-mat/0211134.
- ³⁰ D. Lampakis *et al.*, cond-mat/0105447.